Atmospheric temperature measurements biases on the Antarctic plateau

Christophe Genthon, Delphine Six, Vincent Favier
Laboratoire de Glaciologie et Géophysique de l'Environnement, CNRS/UJF, Saint Martin d'Hères, France

Matthew Lazzara, Linda Keller
Antarctic Meteorological Research Center, University of Wisconsin-Madison, Madison, USA

genthon@lgge.obs.ujf-grenoble.fr

Submitted Atmos. Oceanic. Technol. 13/05/2011

Dome C, Antarctica

Latitude 75°06.06S Longitude 123°20.74E Altitude 3350m

A permanent station, Concordia, jointly operated by the French and Italian polar institutes (IPEV, PNRA)

Dome C selected as a « special site » for CLMIP5 / IPCC AR5

Continuous meteorological profiling system on a 45-m tower since 2008

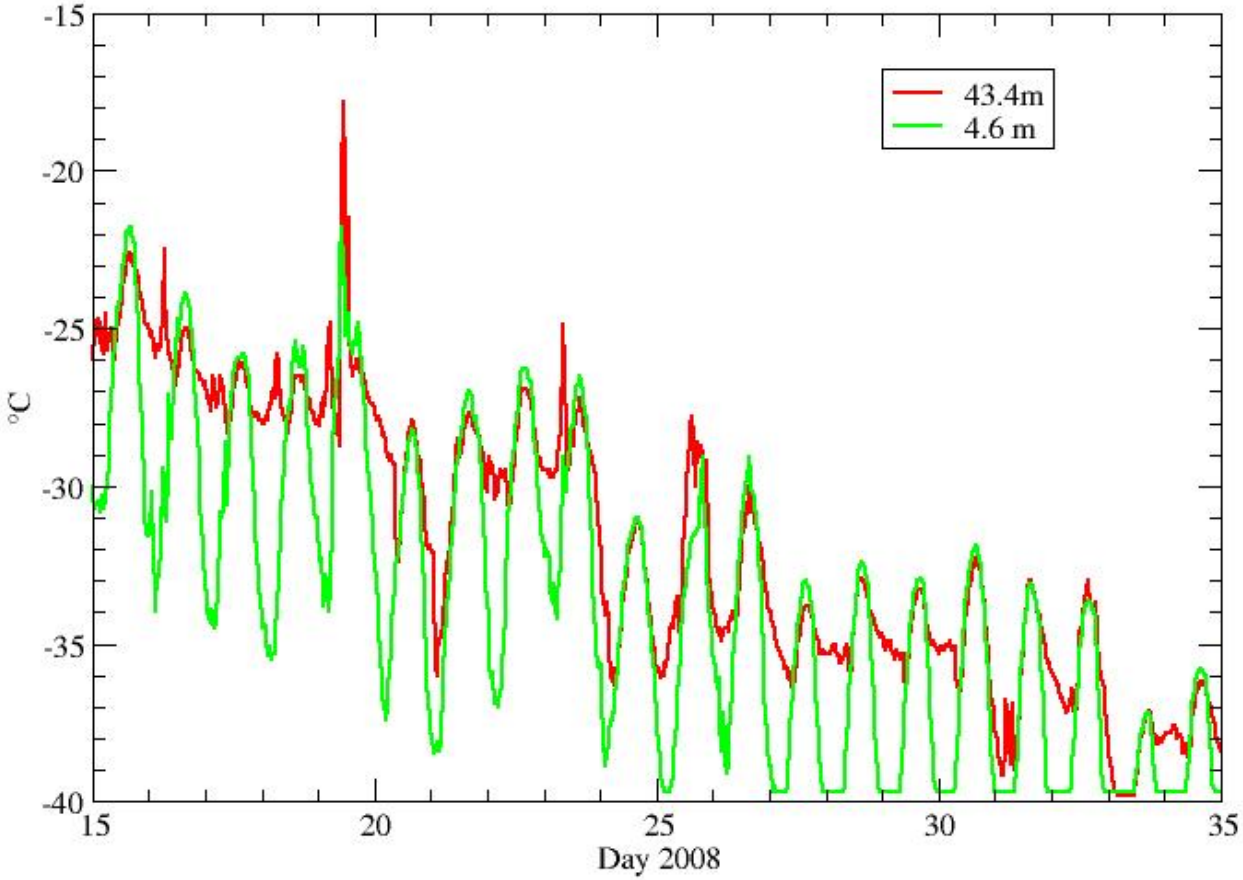

Summer 2008:
- 4 m: Strong diurnal cycle
- 45 m Diurnal cycle strongly damped
- Mid-day: Same temperature => convective mixing

(Genthon et al., J. G. R., 2010)

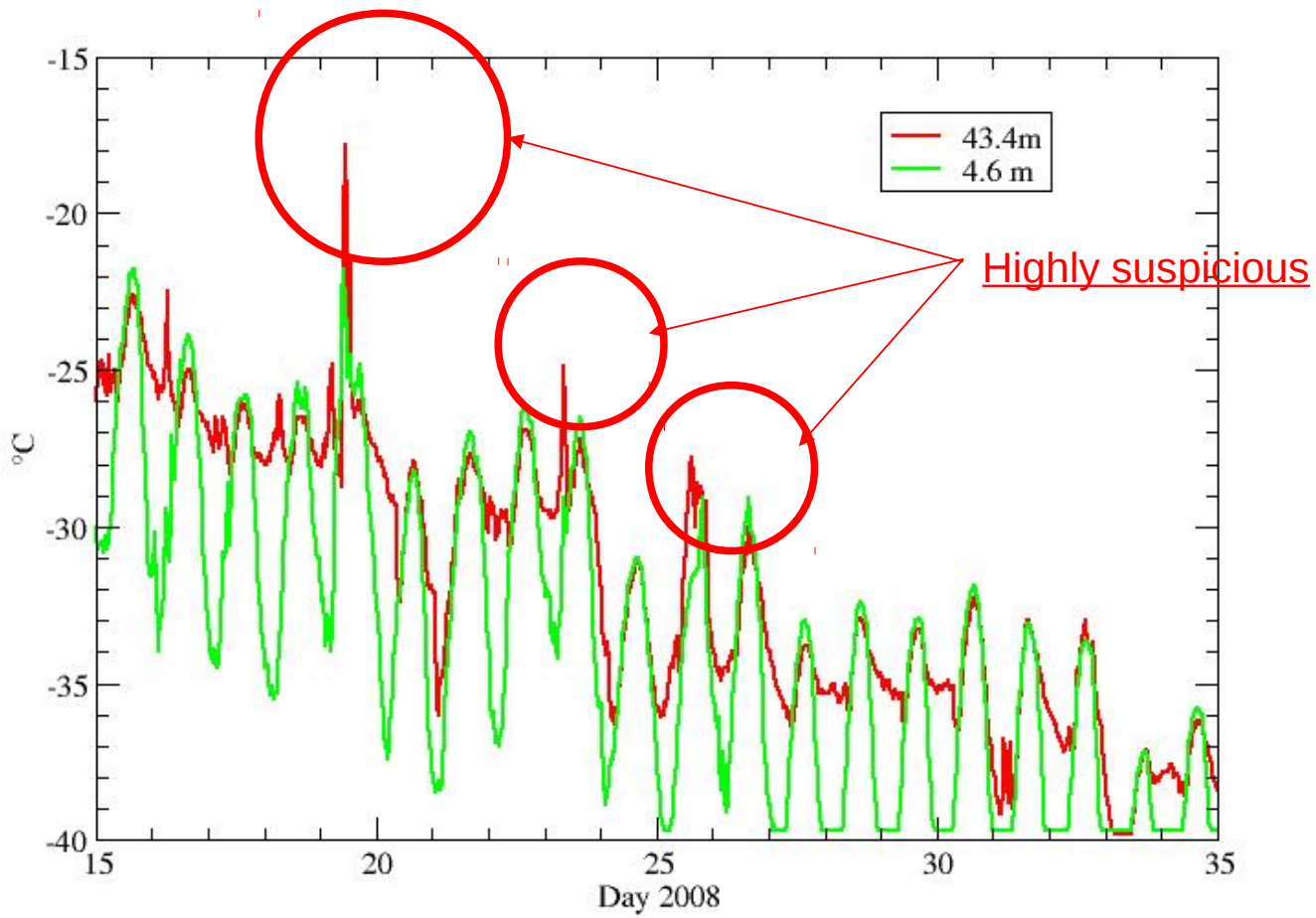

- There are highly suspicious unrealistic warm events in summer
- They occur when wind is weak

In 1873, the Royal Meteorological Society produced a list of conditions that should be fulfilled by a thermometer screen:

1 - The thermometers should be protected from the rays from the sun at all time

2 – The thermometers must be unaffected by the heating of the outside of the screen

3 – Reflected radiation must be excluded

4 – Other external factors (e.g. heat from nearby buildings) must be excluded

5 – There must be free access of the air around the thermometers

6 – The thermometers must not be wet by precipitation

Stevenson screen

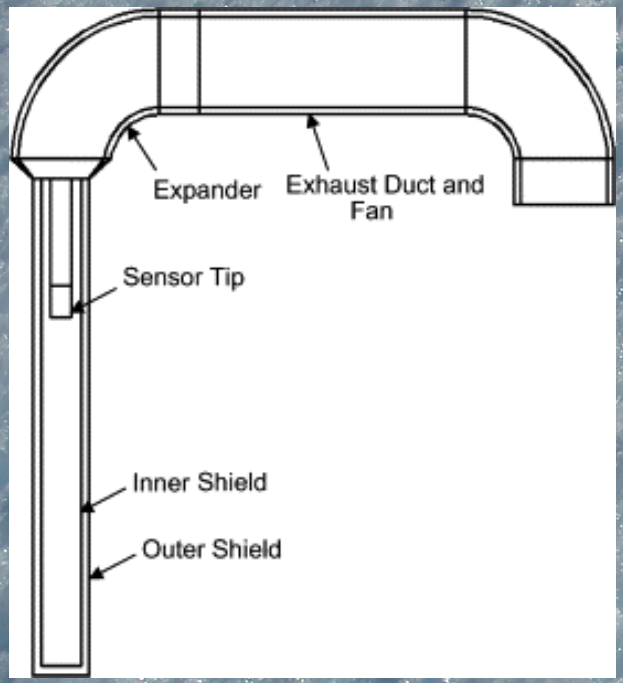

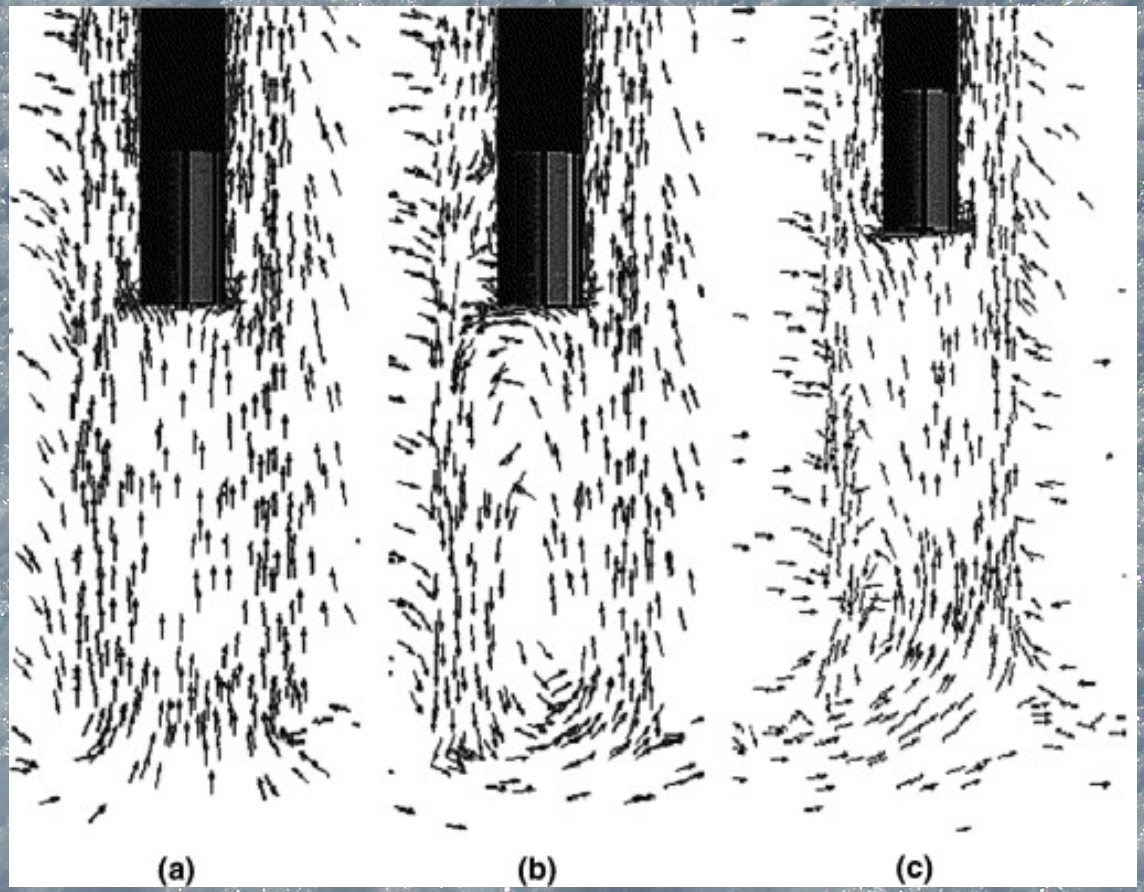

Mahajan et al., 2005. Mechanically aspirated radiation shields: A CFD and neural network design analysis, Int. J. of Heat and Mass Transfer

and by the sensor inside. The program traces rays in two dimensions: *R*, the shield radial, and *Z*, the shield height. This code is limited to radially symmetric, multiplate shields such as the Gill shield, with a cylindrical sensor located along the centerline. The wavelength-dependent shield and/or sensor absorptivity is examined by running the program with various shield and/or sensor absorptivities.

Since a real plate surface is not perfectly smooth, the reflections will not be exactly specular, and, therefore, at each reflection a single ray can be scattered into multiple rays with slightly different angles. To simulate this, a random angle with a Gaussian distribution is added to the calculated specular reflection angle. By launching many different rays from the same location or by launching many closely spaced rays, the program approximates nonspecular reflections. The user specifies the standard deviation of the random angle; if the standard deviation is zero, reflection will be specular. Results are not very sensitive to the choice of the standard deviation.

At each reflection from a surface, a ray losses power equal to its current intensity times the surface absorptivity times the cross-sectional width of the surface. Ray width is taken to be the width of the shield or the width of the sensor.

Rays are launched with source angles ranging from −89° to 89°, where 0° indicates a horizontal ray and 90° is the sun directly overhead. Negative angles indicate radiation reflected from below. Primary program output is the power absorbed by each plate and the power absorbed by the sensor as a function of the source angle. This is modulated by the desired source strength.

A shield with a radiation efficiency of 1.0 does not allow any radiation to reach the sensor, but it will not be a useful design if it blocks airflow. An efficiency of 0.0 indicates the shield is not providing protection. Typical shield efficiencies range from 0.5 to 1.0 and vary considerably as a function of the angle of incidence. Figure 3 is a plot of the calculated radiation efficiency as a function of solar angle for the Gill shield. The plot must be interpreted using some estimate of the relative power density as a function of solar angle.

In an attempt to minimize the flux of solar radiation reaching the sensor, shield N221E was designed. Ray tracing indicated that the radiation efficiency for N221E is better than that for the Gill design; average efficiency for positive angles increased from 0.86 for the Gill to 0.97 for N221E. For negative angles the average efficiency increased from 0.72 for the Gill to 0.91 for N221E. Both shields are most sensitive to radiation coming from negative angles. The amount of energy reflected from below is a function of the ground cover and can be highly reflective for snow and dry sand or rather low over a grass-covered surface.

The ray tracing program was used to map the radiation received along the shield axis, as if the sensor extended all the way from the bottom shield plate to the inside top of the shield. In the shield cross section

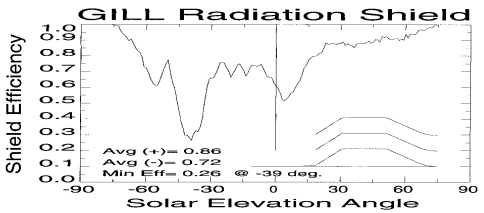

FIG. 3. Calculated radiation efficiency of the Gill shield. The average for positive angles of incident radiation is 0.86 and 0.72 for negative angles.

in Fig. 1a, plates 1–9 dip down near the center but plate 10 does not. Ray tracing showed this causes a radiation ''hot spot'' just below plate 10 because rays entering the shield between plates 9 and 10 can reach the centerline with fewer reflections than rays entering between lower plates.

Tests indicate that for incident rays that do not bounce clear of the shield after the first reflection, the shield acts almost like a blackbody irrespective of the shield absorptivity. Put another way, ray tracing shows that no matter where a ray goes after initial shield entry, on average, most of its energy will be lost to the shield or to the sensor. This is an undesirable characteristic because the radiative energy absorbed by the shield may eventually cause radiational heating errors.

b. Wind tunnel experiments

Two sets of wind tunnel experiments were conducted: one to measure the flow speed inside the shield and another to measure the temperature rise of a sensor inside the shield as a function of external radiational heating and external flow speed. The National Center for Atmospheric Research (NCAR) wind tunnel was used to evaluate the Gill multiplate shield (as built by R. M. Young) and the N221E shield. Airflow inside the shield, on the vertical shield axis, was measured using a Thermo Systems Inc. model 8470 omnidirectional, hot-film air velocity transducer with a 2-mm-diameter sensing head. The wind profile along the shield axis was measured for various external flow rates starting at 1 m s^{-1}. Excess temperature, air temperature inside the shield minus the air temperature at a point upstream from the shield, was measured using YSI 44006 bead thermistors under various wind speed conditions, while illuminating the shield with a strong light source (projecting 630 w m^{-2} on the shield). Both transducer probes were moved ver-

Surface-reflected radiation is a major issue over high-albedo surfaces
(Richardson et al., 1999, J. Atmos. Oceanic Technol.)

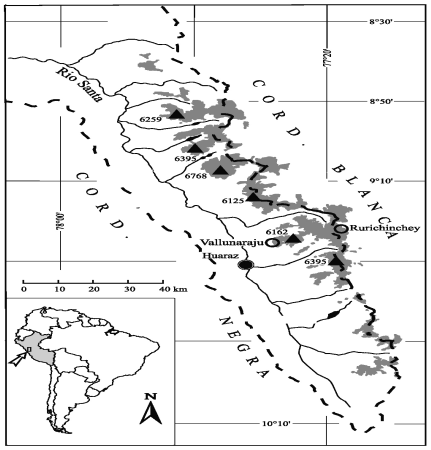

Figure 1. The Cordillera Blanca in northern Perú. Gray shadings show the glacier extents, circles indicate the positions of the automatic weather stations (AWS) close to the respective glaciers. The left-hand side inlay points to the Cordillera Blanca's position in South America.

[11] The sensors are installed 2 m above ground (Table 1), and each was extensively tested and carefully calibrated.

[12] The pyranometers received a 5 week calibration run using a Kipp & Zonen CM 21 pyranometer. The 50Y temperature/humidity probes use 1000 Ω PRTs (DIN 43760B) with a temperature accuracy of 0.3 K, and were calibrated to freezing-point in an ice-water bath. Only for the wind sensors the manufacturers' calibration certificates were considered to be sufficient.

[13] A Campbell Scientific CR 10X data logger controls all devices and stores the processed data as hourly values (Table 2). The sample rate of most sensors is 1 h. Only incoming shortwave radiation and wind speed are sampled at higher rates (3 min) and then processed to 1 hourly means.

[14] Power supply of the station is provided by a 12 V DC pure lead battery (26 Ah). Two 10-W solar panels

Figure 2. The automatic weather station (AWS) on a side ridge of Glaciar Rurichinchey (Cordillera Blanca, Perú) in the approximate altitude of the equilibrium line (Rurichinchey EL). The horizontal support carries the sensors (from left to right): incoming shortwave radiation, temperature/humidity and wind. The background documents the overall environment of the study site. The glacier tongue of Glaciar Rurichinchey is shown on the right side, the arrow labels the position of the glacier forefield AWS (Rurichinchey FF), which actually stands slightly behind the ridge. See color version of this figure at back of this issue.

recharge the battery via a regulator. The largest power consumer of the system is the ventilation fan. The ventilation is not switched on in case of low battery voltage. This guarantees the continuous operation of the logger and all sensors.

2.3. Ventilated and Unventilated Measurements

[15] The custom-made radiation shield containing the temperature/humidity probe consists of two plastic tubes fit into each other (outer tube: ↕ 30 cm, Ø 15 cm, Figure 3). The top of this vertically mounted double tube is protected by a cover wider in diameter (Ø 17 cm), which overlaps the tube. The inner tube is completely shielded from direct solar radiation by the outer one and a closed bottom. The probe is placed in the upper part of the tube. An electric fan is mounted on top of the inner tube (3.5 ms^{-1}) and sucks the air from bottom to top. Air flow is ensured by big holes in the lower part of the inner tube. The closed design of the radiation shield provides protection for the sensor and the

Table 1. Sensors Installed at the Cordillera Blanca Automatic Weather Stations

Variable	Sensor (Manufacturer, Model)
Wind speed	R.M. Young 05103
Wind direction	
Incoming shortwave radiation	Schenk star pyranometer 8101
Air temperature	Vaisala 50 Y
Relative humidity	

Table 2. Measurements and Sampling Rates of the Cordillera Blanca Automatic Weather Stations

Variable		Sampling Rate	Data Stored
Air temperature	vent.	1 hour	1 hour (actual value)
	unvent.	1 hour*	1 hour (actual value)
Relative humidity	vent.	1 hour	1 hour (actual value)
	unvent.	1 hour*	1 hour (actual value)
Incoming shortwave radiation		3 min	1 hour (mean)
Wind speed		3 min	1 hour (mean)
		1 hour	1 hour (actual value)
Wind direction		1 hour	1 hour (actual value)

*Unventilated measurements 6 min earlier than ventilated ones.

electric fan, which is advantageous due to the unattended operation. After 54 min of no ventilation, the unventilated sample is taken and ventilation is switched on. At the end of the 6 min ventilation period the ventilated sample is logged, the fan is switched off and the procedure starts again. Ventilation switch-offs/failures can be screened in the stored data by the logged fan rotation frequency.

[16] The measuring of both temperatures with the same probe and shield at the same place overcomes common calibration problems of the usual setup with two independent probes and shields [*Harding et al.*, 1987; *Hock*, 1994; *Hardy et al.*, 1998]; deviations resulting from the use of different probes, shields or locations are completely avoided.

[17] The 6 min gap may possibly result in unsystematic errors between single unventilated and ventilated temperature pairs. However, the purpose of the AWSs is to gain climatological information. For these statistical values (like daily means or daily cycles per month) these errors minimize. The considerations presented here only deal with such statistical values.

3. Analysis of Ventilated and Unventilated Temperature Data

[18] The AWS data cover the time from from October 1999 until May 2001. The Rurichinchey FF (glacier forefield) and Vallunaraju AWSs performed very satisfying. There are no periods of missing data at either station. The Rurichinchey FF series consists of 14208 hourly samples, starting on 24 September 1999 and ending on 07 May 2001 so far. Only three samples have turned-off or low ventilation, which is 0.02%. Samples are considered to have low ventilated if airspeed is below 2.5 ms^{-1}. The Vallunaraju AWS series is 9048 hourly samples (09 May 2000–20 May 2001). There were more turned-off/low ventilation samples (238 samples or 3.5%) until February 2001, which is still an acceptable value. Ventilation stopped unexpectedly on 13 February 2001, presumably due to a mechanical failure of the fan.

[19] The Rurichinchey FF AWS serves for the following data analysis of unventilated versus ventilated temperature samples and the development of the correction model, since it is influenced very seldomly by snow-covered ground. There are very few snow fall events due to the low altitude of the station. In these cases, the snow melts within hours.

[20] Averaging over the whole observational period the ventilated temperature at Rurichinchey FF is 1.9°C, whereas the unventilated one is 2.6°C. The unventilated mean exceeds the ventilated one by 0.7 K.

[21] Deviations of hourly $\Delta T = T_{unvent.} - T_{vent.}$ samples are found from −2.3 to +7.6 K. Daily mean differences range from 0.2 to 1.2 K, monthly difference means from 0.64 to 0.75 K. The values correspond to those of *Hardy et al.* [1998], *Harding et al.* [1987] and *Hock* [1994], although the Rurichinchey FF AWS is seldom influenced by reflection from snow/ice-covered surface. The steadiness of the ΔT monthly means throughout the year is remarkable, even regarding the all-year round constant temperatures. It provides suitable boundary conditions for the correction.

[22] The extent of temperature difference depends on shortwave radiation, longwave radiation and turbulent energy fluxes affecting the outside of the shield. Thus it may be attributed to the respective fluxes. Incoming short-

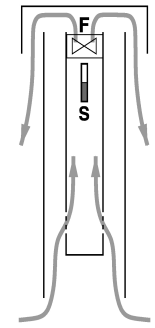

Figure 3. Sketch of the custom-made radiation shield for the temperature/humidity probe. An electric fan (F) sucks air from bottom to top, the sensor (S) is mounted below the fan.

George and Kaser, 2002; Ventilated and unventilated air-temperature measurements for glacier-climate studies on a tropical high mountain site, JGR.

Huwald et al, 2009: Albedo effect on radiative errors in air measurements, Water Resour. Res.

2009 on: Aspirated (RM Young 43502)
Forced Ventilation = FV

2008: Gill-styled multiplate (Campbell URS)
Natural Ventilation = NV

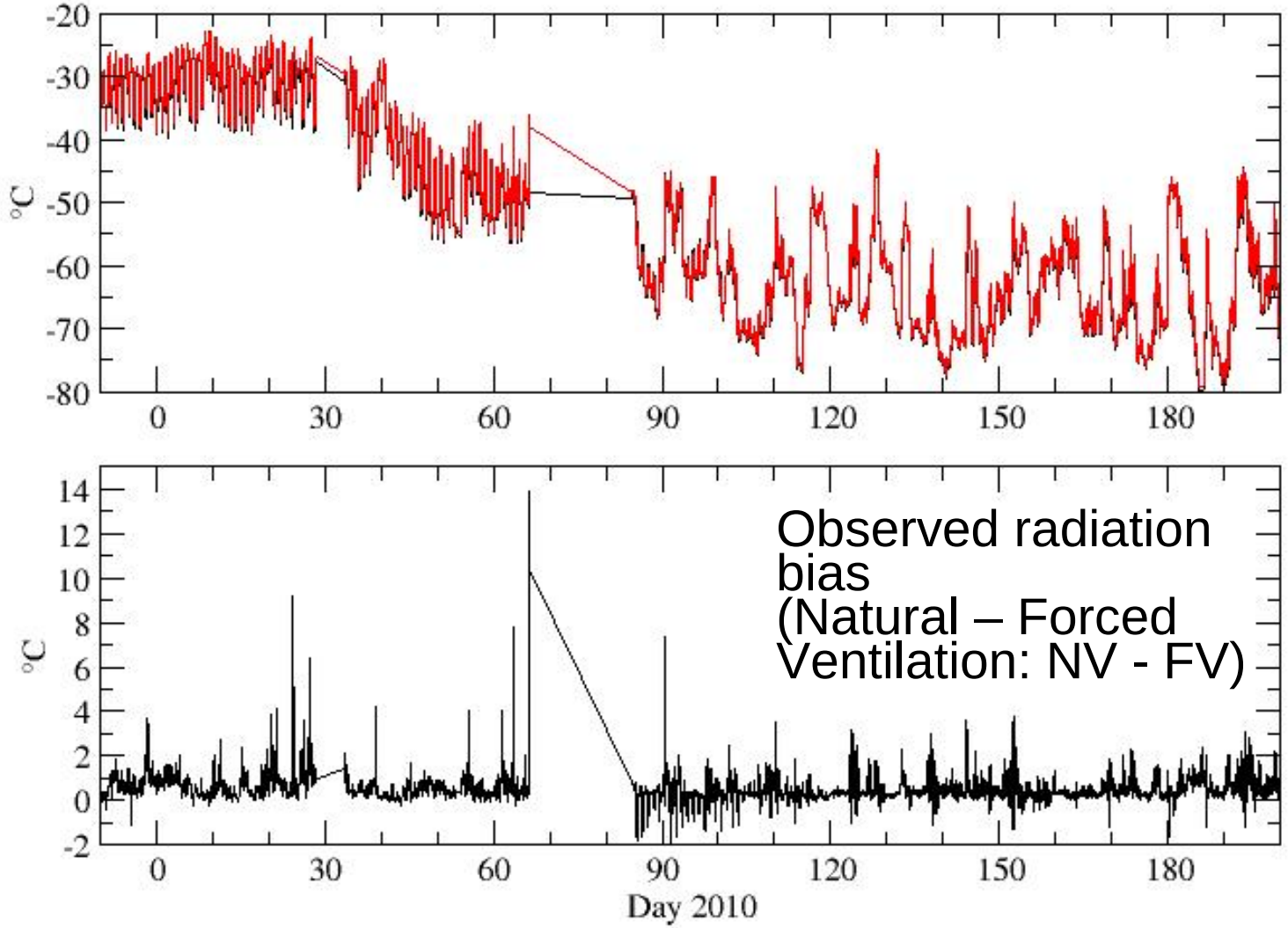
-20
-30
-40
-50
-60
-70
-80
°C
0
30
60
90
120
150
180
14
12
10
8
6
4
2
0
-2
°C
Observed radiation bias
(Natural – Forced Ventilation: NV - FV)
Day 2010

In principle, sonic thermometers (SO) are unaffected by radiation. However, they are
- Much more expensive (than e.g. PT100)
- Tricky, sensitive
- Energy consuming

NV : Natural ventilation ; **FV** : Forced ventilation (aspirated) ; **SO** : Sonic

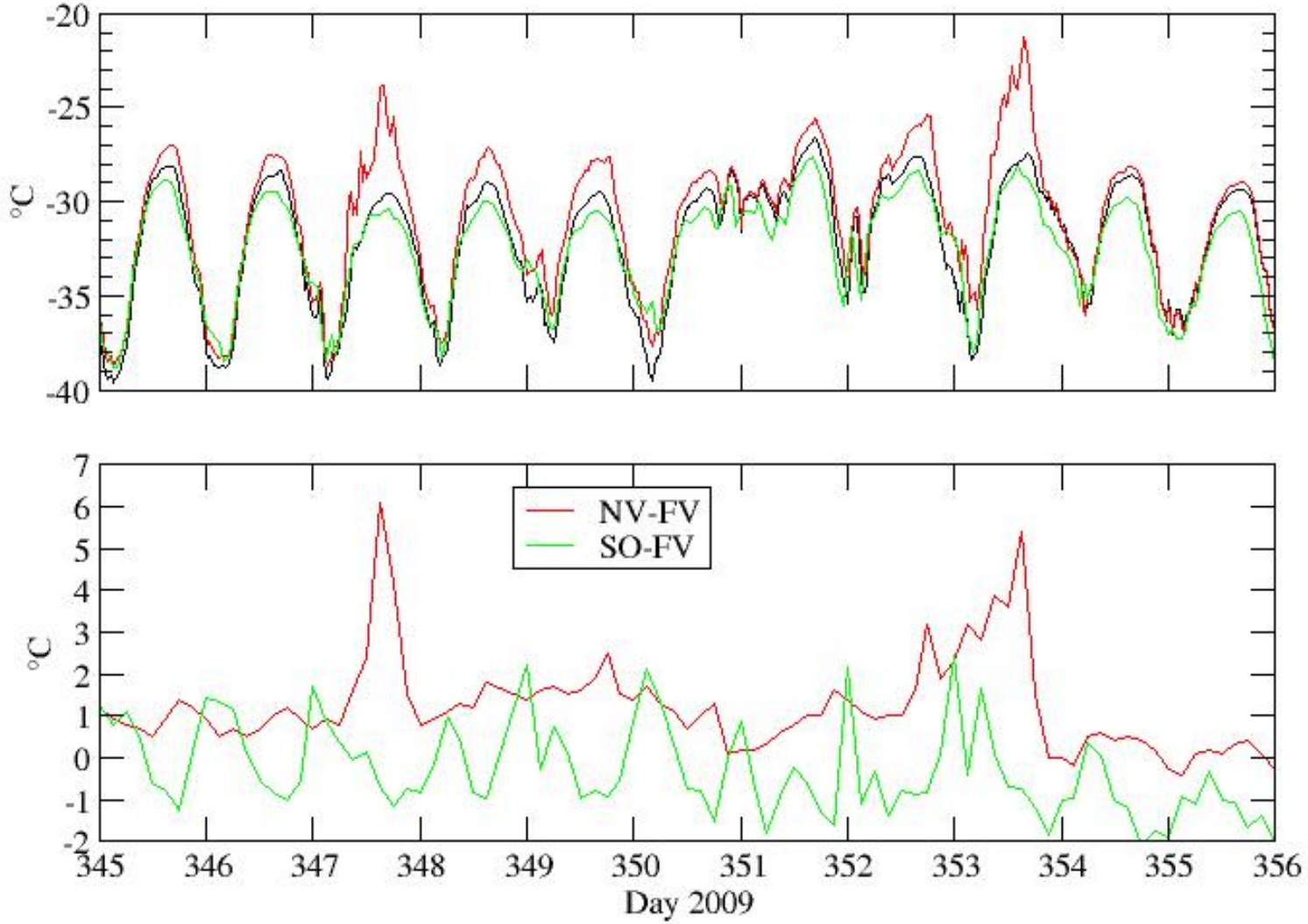

Radiation bias (NV-FV) versus..

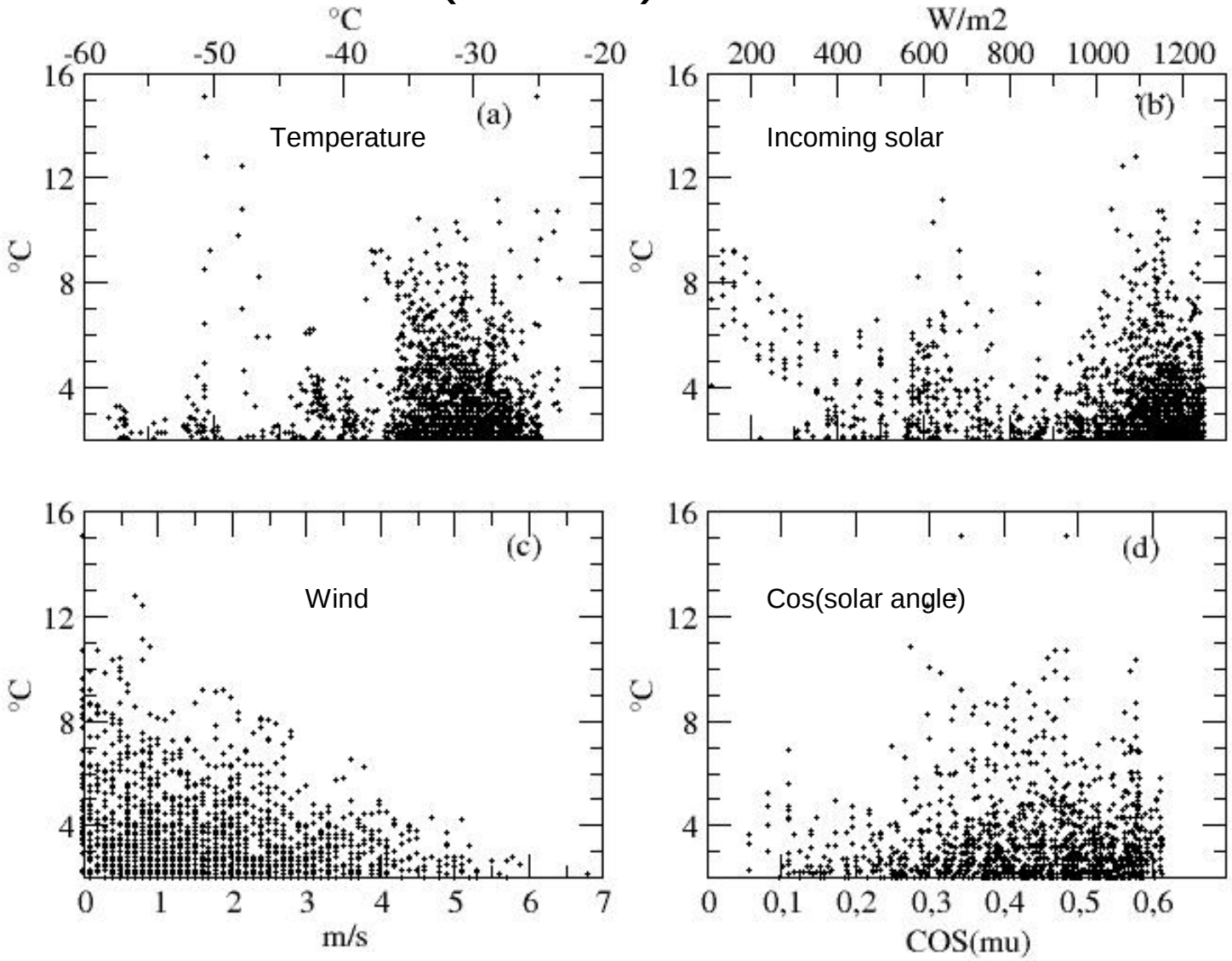

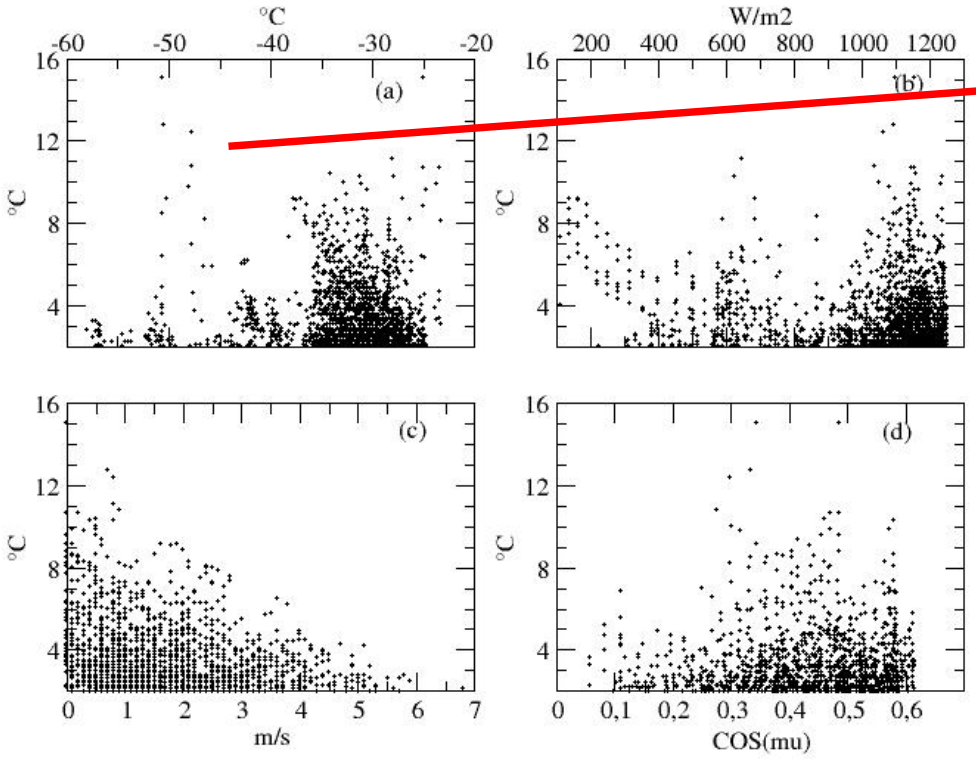

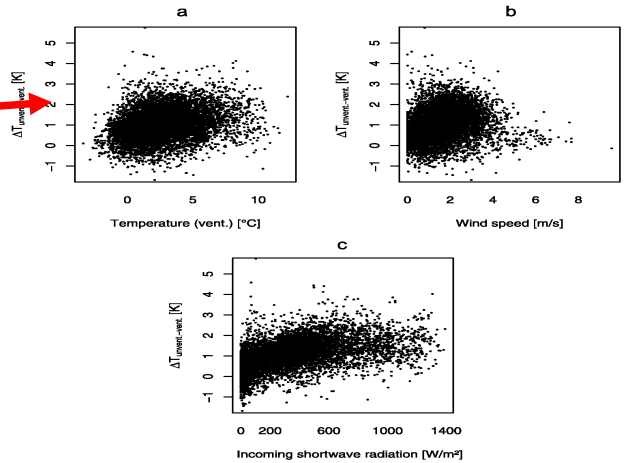

Figure 4. Scatterplots of temperature difference (unventilated-ventilated) versus ventilated temperature (a), wind speed (b) and incoming shortwave radiation (c) at Rurichinchey FF AWS for the period 24 September 1999–07 May 2001.

wave radiation is measured, ventilated temperature samples may give information on the long wave fluxes resulting from thermal radiation of the surrounding atmosphere and wind speed samples may be looked at as a parameter indicating the turbulent fluxes due to (air) mass flow to the radiation shield. In Figure 4 the respective scatterplots are shown. Whereas the scatters of ventilated temperature versus temperature difference (Figure 4a) and wind speed versus temperature difference (Figure 4b) do not support any statistical association, there exists a certain statistical relation for incoming shortwave radiation and temperature difference (Figure 4c). Correction approaches using simple linear correlations are not satisfactory due to large scattering (Figure 4c). The correlation coefficient for a linear correlation of incoming shortwave radiation versus temperature difference is $r = 0.55$, multiple correlations including ventilated temperature and/or wind speed raise r only little due to the low statistical association (Figures 4a and 4b).

[23] The comparison of mean daily cycles of temperature difference and incoming shortwave radiation may reveal the generally low correlations (Figure 5). The daily run of ΔT consists of two plateau situations: one of about 0.3 K during the night and another of 1.3 K during daytime. The daytime plateau shows slight maxima in late morning and early afternoon and a slight minimum at noon. It is nearly symmetrical for morning and afternoon with the axis of symmetry at noon. The step-like changes from night to day and vice versa occur within 2–3 hours. This daily cycle of ΔT is in good agreement with those measured by *Anderson and Baumgartner* [1998] in tropical seas. The daytime cycle of incoming shortwave radiation on Rurichinchey is nearly symmetrical for morning and afternoon as well, but has only one maximum of 600 Wm^{-2} at noon. Although the differences of the daily cycles of incoming shortwave radiation and ΔT are slight, they are responsible for the unsatisfying correlation between the parameters. Nevertheless, the only encouraging correlation is with incoming shortwave radiation and other reasons for the temperature differences are unlikely.

4. A Simple Radiation Geometry Model

[24] Regarding the previous discussion, a simple radiation geometry model is proposed for an explanation of ΔT. The

Our work (Antarctic plateau)

Georges and Kaser 2002 (tropical glacier)

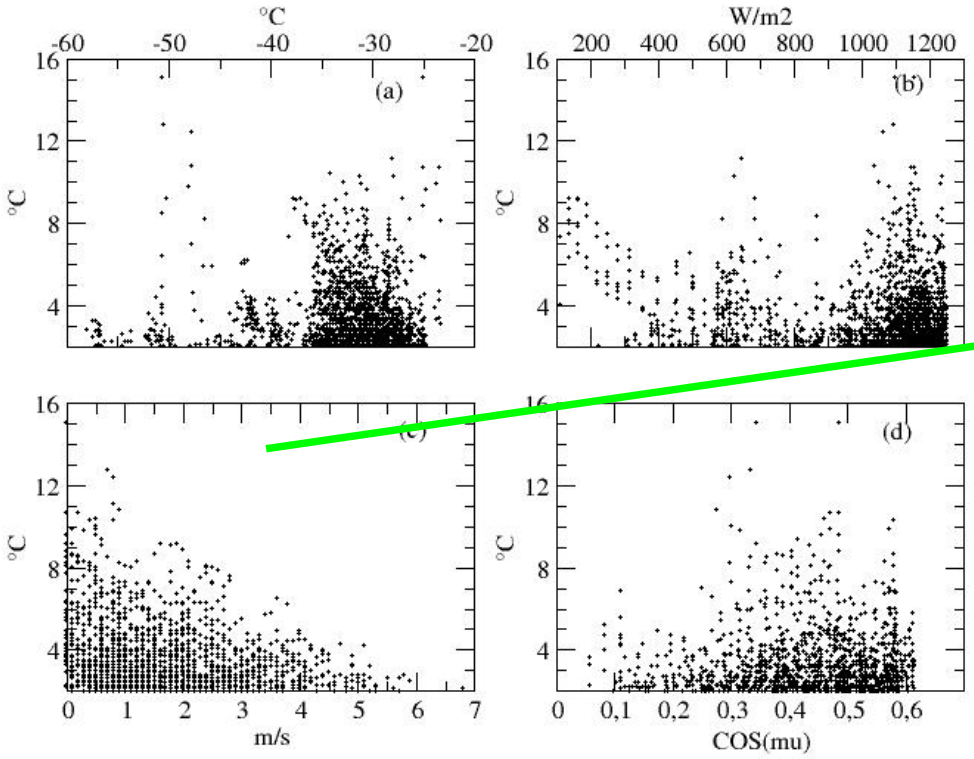

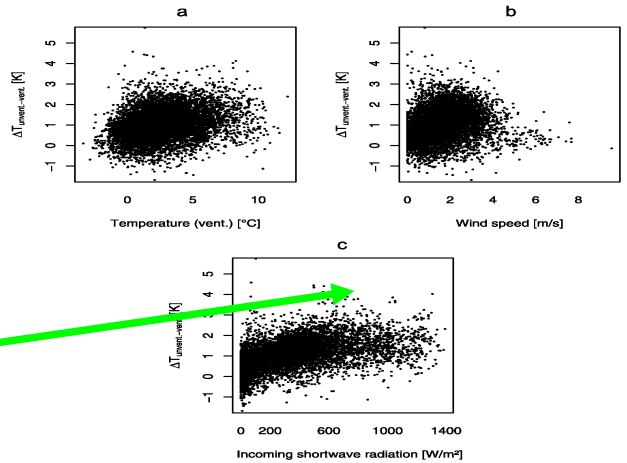

Figure 4. Scatterplots of temperature difference (unventilated-ventilated) versus ventilated temperature (a), wind speed (b) and incoming shortwave radiation (c) at Rurichinchey FF AWS for the period 24 September 1999–07 May 2001.

wave radiation is measured, ventilated temperature samples may give information on the long wave fluxes resulting from thermal radiation of the surrounding atmosphere and wind speed samples may be looked at as a parameter indicating the turbulent fluxes due to (air) mass flow to the radiation shield. In Figure 4 the respective scatterplots are shown. Whereas the scatters of ventilated temperature versus temperature difference (Figure 4a) and wind speed versus temperature difference (Figure 4b) do not support any statistical association, there exists a certain statistical relation for incoming shortwave radiation and temperature difference (Figure 4c). Correction approaches using simple linear correlations are not satisfactory due to large scattering (Figure 4c). The correlation coefficient for a linear correlation of incoming shortwave radiation versus temperature difference is $r = 0.55$, multiple correlations including ventilated temperature and/or wind speed raise r only little due to the low statistical association (Figures 4a and 4b).

[23] The comparison of mean daily cycles of temperature difference and incoming shortwave radiation may reveal the generally low correlations (Figure 5). The daily run of ΔT consists of two plateau situations: one of about 0.3 K during the night and another of 1.3 K during daytime. The daytime plateau shows slight maxima in late morning and early afternoon and a slight minimum at noon. It is nearly symmetrical for morning and afternoon with the axis of symmetry at noon. The step-like changes from night to day and vice versa occur within 2–3 hours. This daily cycle of ΔT is in good agreement with those measured by *Anderson and Baumgartner* [1998] in tropical seas. The daytime cycle of incoming shortwave radiation on Rurichinchey is nearly symmetrical for morning and afternoon as well, but has only one maximum of 600 Wm^{-2} at noon. Although the differences of the daily cycles of incoming shortwave radiation and ΔT are slight, they are responsible for the unsatisfying correlation between the parameters. Nevertheless, the only encouraging correlation is with incoming shortwave radiation and other reasons for the temperature differences are unlikely.

4. A Simple Radiation Geometry Model

[24] Regarding the previous discussion, a simple radiation geometry model is proposed for an explanation of ΔT. The

Our work (Antarctic plateau)

Georges and Kaser 2002 (tropical glacier)

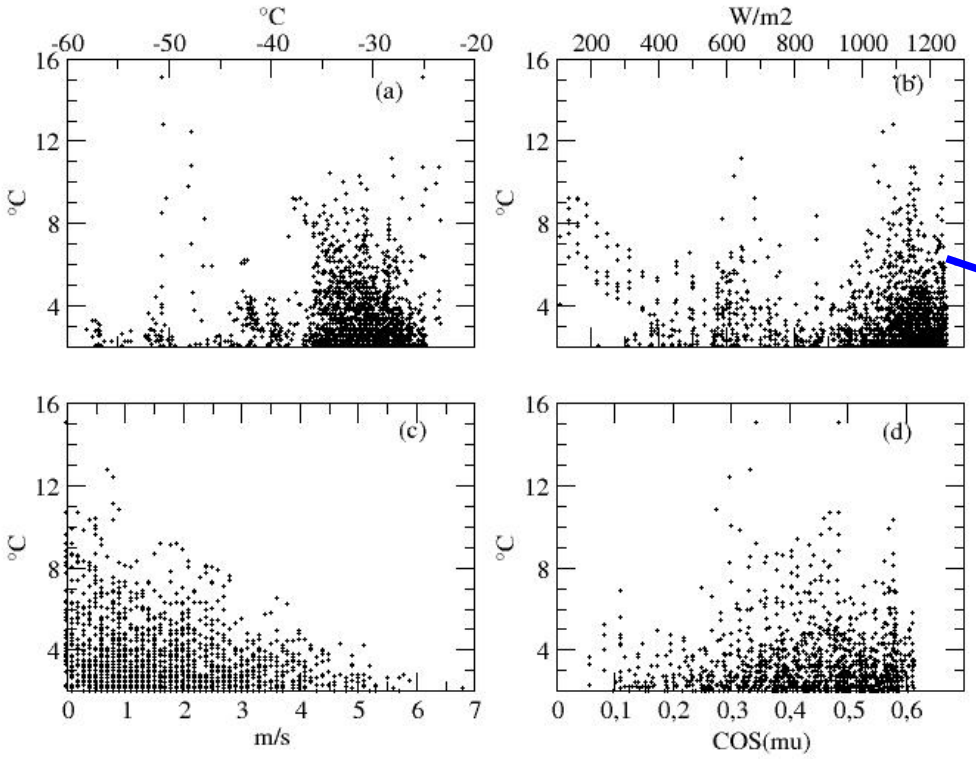

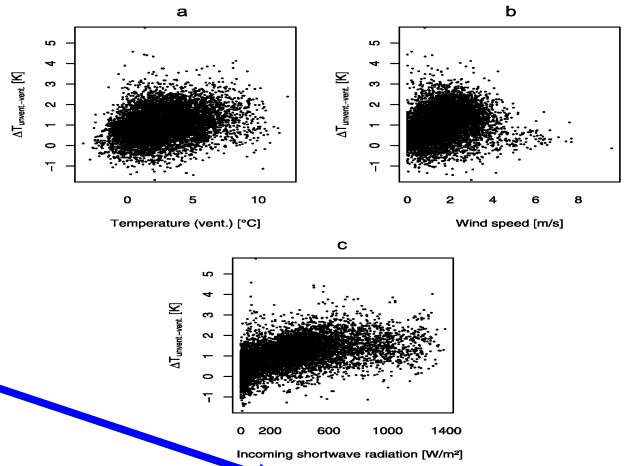

Figure 4. Scatterplots of temperature difference (unventilated-ventilated) versus ventilated temperature (a), wind speed (b) and incoming shortwave radiation (c) at Rurichinchey FF AWS for the period 24 September 1999–07 May 2001.

wave radiation is measured, ventilated temperature samples may give information on the long wave fluxes resulting from thermal radiation of the surrounding atmosphere and wind speed samples may be looked at as a parameter indicating the turbulent fluxes due to (air) mass flow to the radiation shield. In Figure 4 the respective scatterplots are shown. Whereas the scatters of ventilated temperature versus temperature difference (Figure 4a) and wind speed versus temperature difference (Figure 4b) do not support any statistical association, there exists a certain statistical relation for incoming shortwave radiation and temperature difference (Figure 4c). Correction approaches using simple linear correlations are not satisfactory due to large scattering (Figure 4c). The correlation coefficient for a linear correlation of incoming shortwave radiation versus temperature difference is $r = 0.55$, multiple correlations including ventilated temperature and/or wind speed raise r only little due to the low statistical association (Figures 4a and 4b).

[23] The comparison of mean daily cycles of temperature difference and incoming shortwave radiation may reveal the generally low correlations (Figure 5). The daily run of ΔT consists of two plateau situations: one of about 0.3 K during the night and another of 1.3 K during daytime. The daytime plateau shows slight maxima in late morning and early afternoon and a slight minimum at noon. It is nearly symmetrical for morning and afternoon with the axis of symmetry at noon. The step-like changes from night to day and vice versa occur within 2–3 hours. This daily cycle of ΔT is in good agreement with those measured by *Anderson and Baumgartner* [1998] in tropical seas. The daytime cycle of incoming shortwave radiation on Rurichinchey is nearly symmetrical for morning and afternoon as well, but has only one maximum of 600 Wm^{-2} at noon. Although the differences of the daily cycles of incoming shortwave radiation and ΔT are slight, they are responsible for the unsatisfying correlation between the parameters. Nevertheless, the only encouraging correlation is with incoming shortwave radiation and other reasons for the temperature differences are unlikely.

4. A Simple Radiation Geometry Model

[24] Regarding the previous discussion, a simple radiation geometry model is proposed for an explanation of ΔT. The

Our work (Antarctic plateau)

Georges and Kaser 2002 (tropical glacier)

Solar angle issue on a highly reflective surface

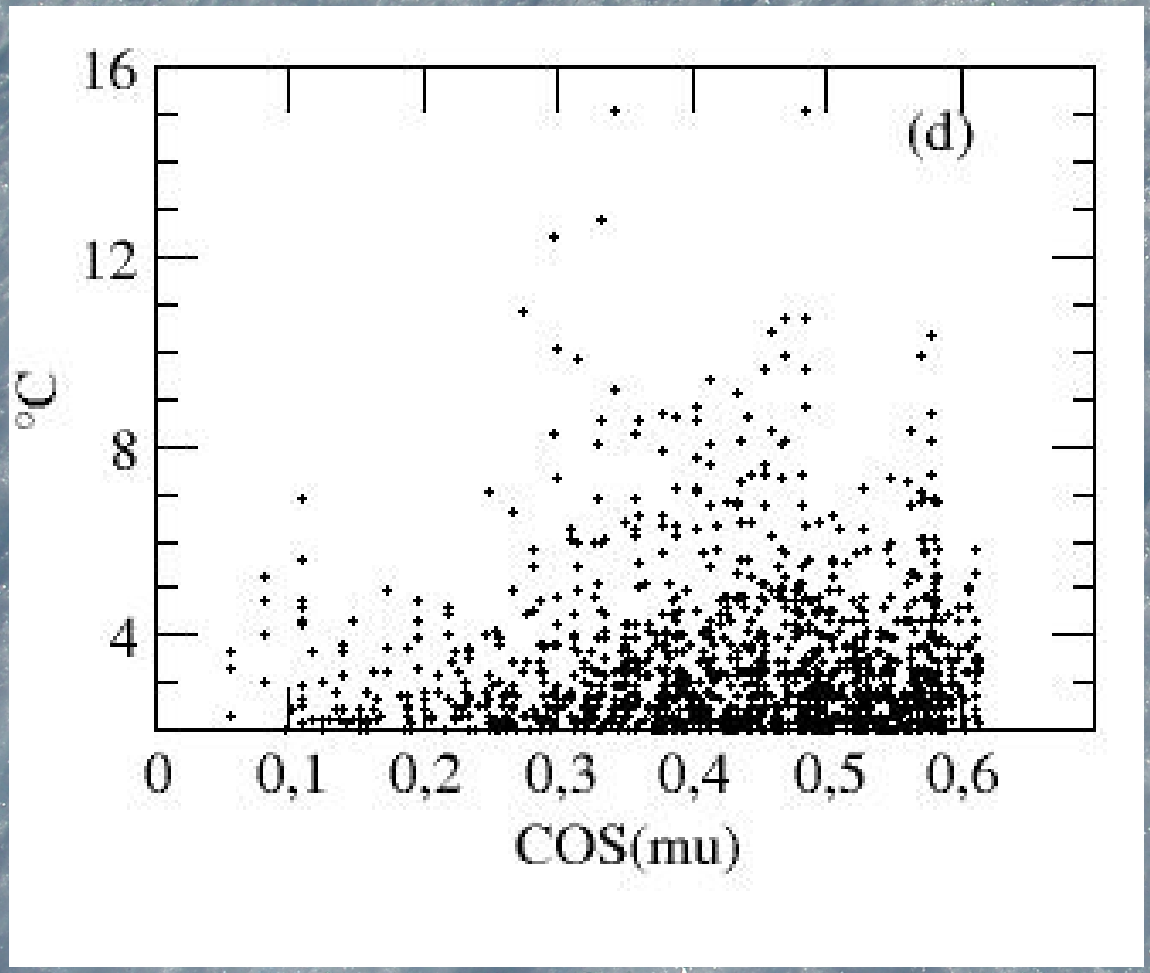

and by the sensor inside. The program traces rays in two dimensions: *R*, the shield radial, and *Z*, the shield height. This code is limited to radially symmetric, multiplate shields such as the Gill shield, with a cylindrical sensor located along the centerline. The wavelength-dependent shield and/or sensor absorptivity is examined by running the program with various shield and/or sensor absorptivities.

Since a real plate surface is not perfectly smooth, the reflections will not be exactly specular, and, therefore, at each reflection a single ray can be scattered into multiple rays with slightly different angles. To simulate this, a random angle with a Gaussian distribution is added to the calculated specular reflection angle. By launching many different rays from the same location or by launching many closely spaced rays, the program approximates nonspecular reflections. The user specifies the standard deviation of the random angle; if the standard deviation is zero, reflection will be specular. Results are not very sensitive to the choice of the standard deviation.

At each reflection from a surface, a ray losses power equal to its current intensity times the surface absorptivity times the cross-sectional width of the surface. Ray width is taken to be the width of the shield or the width of the sensor.

Rays are launched with source angles ranging from −89° to 89°, where 0° indicates a horizontal ray and 90° is the sun directly overhead. Negative angles indicate radiation reflected from below. Primary program output is the power absorbed by each plate and the power absorbed by the sensor as a function of the source angle. This is modulated by the desired source strength.

A shield with a radiation efficiency of 1.0 does not allow any radiation to reach the sensor, but it will not be a useful design if it blocks airflow. An efficiency of 0.0 indicates the shield is not providing protection. Typical shield efficiencies range from 0.5 to 1.0 and vary considerably as a function of the angle of incidence. Figure 3 is a plot of the calculated radiation efficiency as a function of solar angle for the Gill shield. The plot must be interpreted using some estimate of the relative power density as a function of solar angle.

In an attempt to minimize the flux of solar radiation reaching the sensor, shield N221E was designed. Ray tracing indicated that the radiation efficiency for N221E is better than that for the Gill design; average efficiency for positive angles increased from 0.86 for the Gill to 0.97 for N221E. For negative angles the average efficiency increased from 0.72 for the Gill to 0.91 for N221E. Both shields are most sensitive to radiation coming from negative angles. The amount of energy reflected from below is a function of the ground cover and can be highly reflective for snow and dry sand or rather low over a grass-covered surface.

The ray tracing program was used to map the radiation received along the shield axis, as if the sensor extended all the way from the bottom shield plate to the inside top of the shield. In the shield cross section

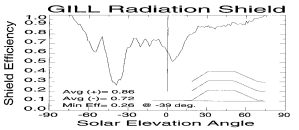

FIG. 3. Calculated radiation efficiency of the Gill shield. The average for positive angles of incident radiation is 0.86 and 0.72 for negative angles.

in Fig. 1a, plates 1–9 dip down near the center but plate 10 does not. Ray tracing showed this causes a radiation "hot spot" just below plate 10 because rays entering the shield between plates 9 and 10 can reach the centerline with fewer reflections than rays entering between lower plates.

Tests indicate that for incident rays that do not bounce clear of the shield after the first reflection, the shield acts almost like a blackbody irrespective of the shield absorptivity. Put another way, ray tracing shows that no matter where a ray goes after initial shield entry, on average, most of its energy will be lost to the shield or to the sensor. This is an undesirable characteristic because the radiative energy absorbed by the shield may eventually cause radiational heating errors.

b. Wind tunnel experiments

Two sets of wind tunnel experiments were conducted: one to measure the flow speed inside the shield and another to measure the temperature rise of a sensor inside the shield as a function of external radiational heating and external flow speed. The National Center for Atmospheric Research (NCAR) wind tunnel was used to evaluate the Gill multiplate shield (as built by R. M. Young) and the N221E shield. Airflow inside the shield, on the vertical shield axis, was measured using a Thermo Systems Inc. model 8470 omnidirectional, hot-film air velocity transducer with a 2-mm-diameter sensing head. The wind profile along the shield axis was measured for various external flow rates starting at 1 m s^{-1}. Excess temperature, air temperature inside the shield minus the air temperature at a point upstream from the shield, was measured using YSI 44006 bead thermistors under various wind speed conditions, while illuminating the shield with a strong light source (projecting 630 w m^{-2} on the shield). Both transducer probes were moved ver-

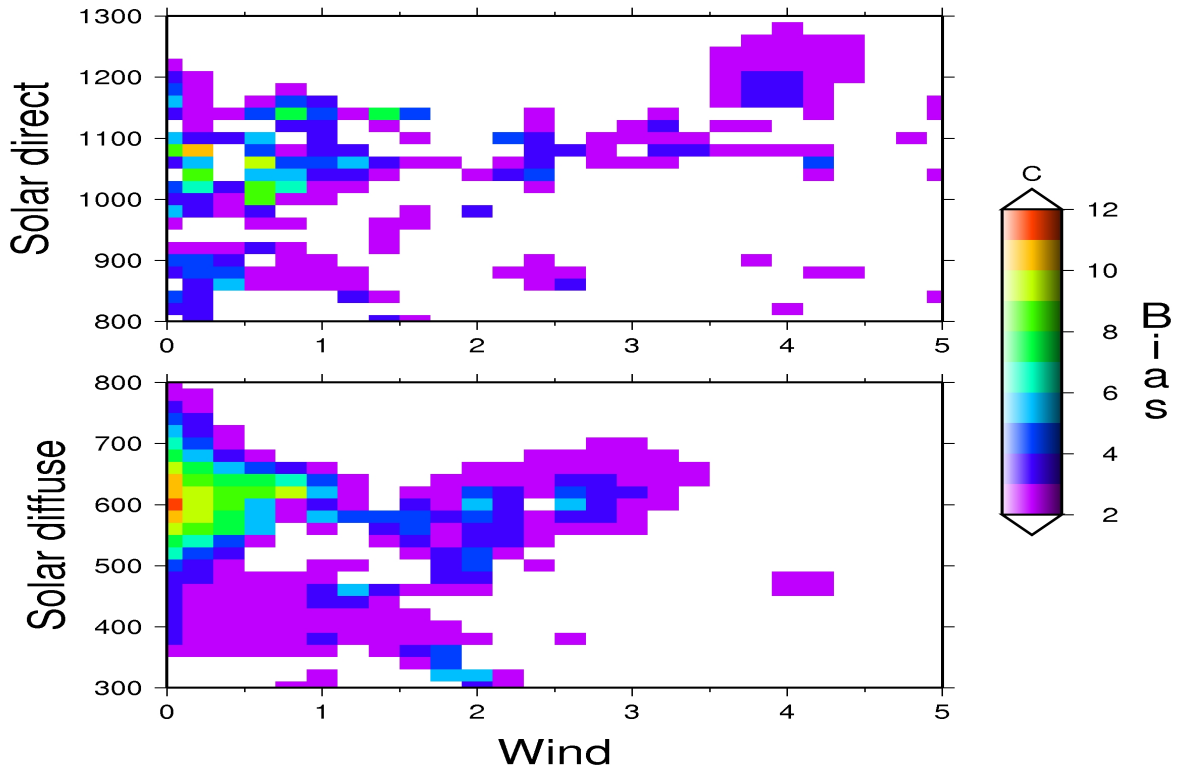

Beware of diffuse (cloudy conditions): Even though absolute radiative flux is less, bias potential is still large

Bias correction? CFD modeling (Mahajan et al. 2005), ray-tracing modeling (Richardson et al. 1999)

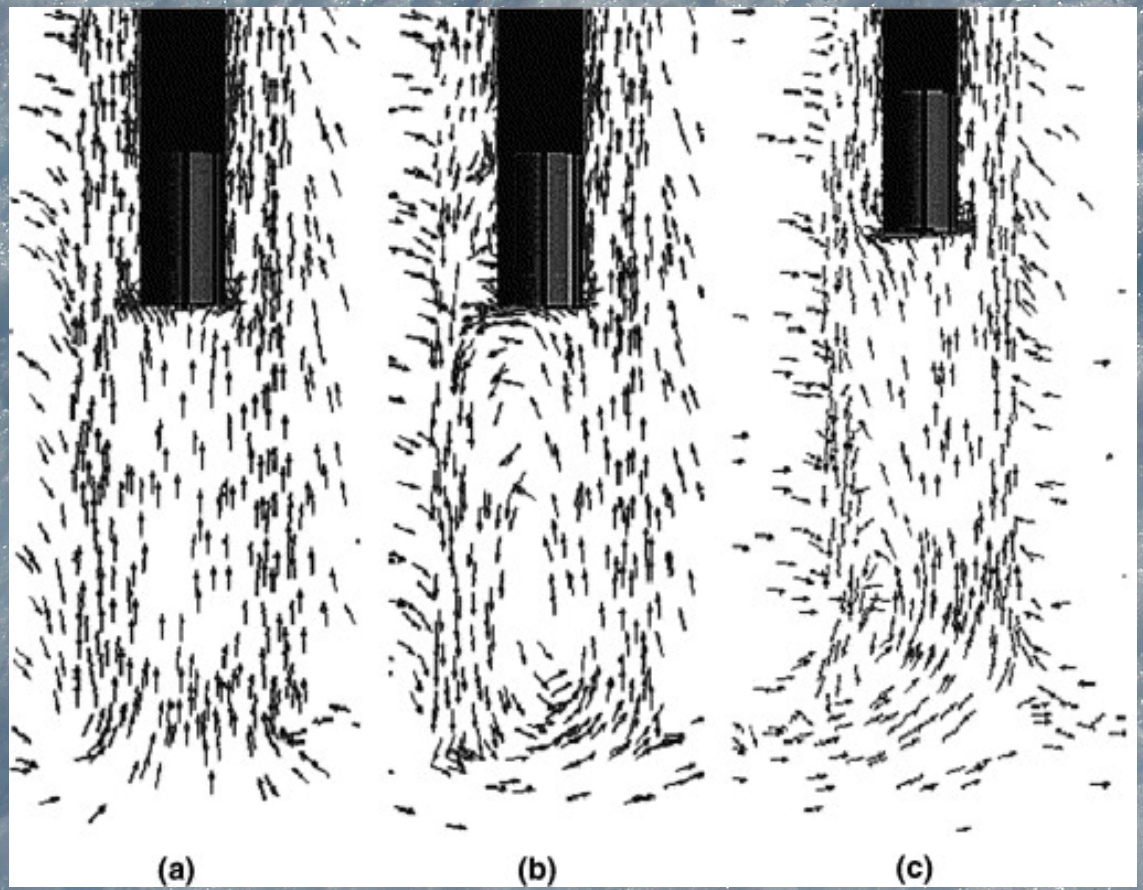

and by the sensor inside. The program traces rays in two dimensions: *R*, the shield radial, and *Z*, the shield height. This code is limited to radially symmetric, multiplate shields such as the Gill shield, with a cylindrical sensor located along the centerline. The wavelength-dependent shield and/or sensor absorptivity is examined by running the program with various shield and/or sensor absorptivities.

Since a real plate surface is not perfectly smooth, the reflections will not be exactly specular, and, therefore, at each reflection a single ray can be scattered into multiple rays with slightly different angles. To simulate this, a random angle with a Gaussian distribution is added to the calculated specular reflection angle. By launching many different rays from the same location or by launching many closely spaced rays, the program approximates nonspecular reflections. The user specifies the standard deviation of the random angle; if the standard deviation is zero, reflection will be specular. Results are not very sensitive to the choice of the standard deviation.

At each reflection from a surface, a ray losses power equal to its current intensity times the surface absorptivity times the cross-sectional width of the surface. Ray width is taken to be the width of the shield or the width of the sensor.

Rays are launched with source angles ranging from −89° to 89°, where 0° indicates a horizontal ray and 90° is the sun directly overhead. Negative angles indicate radiation reflected from below. Primary program output is the power absorbed by each plate and the power absorbed by the sensor as a function of the source angle. This is modulated by the desired source strength.

A shield with a radiation efficiency of 1.0 does not allow any radiation to reach the sensor, but it will not be a useful design if it blocks airflow. An efficiency of 0.0 indicates the shield is not providing protection. Typical shield efficiencies range from 0.5 to 1.0 and vary considerably as a function of the angle of incidence. Figure 3 is a plot of the calculated radiation efficiency as a function of solar angle for the Gill shield. The plot must be interpreted using some estimate of the relative power density as a function of solar angle.

In an attempt to minimize the flux of solar radiation reaching the sensor, shield N221E was designed. Ray tracing indicated that the radiation efficiency for N221E is better than that for the Gill design; average efficiency for positive angles increased from 0.86 for the Gill to 0.97 for N221E. For negative angles the average efficiency increased from 0.72 for the Gill to 0.91 for N221E. Both shields are most sensitive to radiation coming from negative angles. The amount of energy reflected from below is a function of the ground cover and can be highly reflective for snow and dry sand or rather low over a grass-covered surface.

The ray tracing program was used to map the radiation received along the shield axis, as if the sensor extended all the way from the bottom shield plate to the inside top of the shield. In the shield cross section

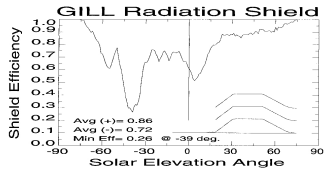

FIG. 3. Calculated radiation efficiency of the Gill shield. The average for positive angles of incident radiation is 0.86 and 0.72 for negative angles.

in Fig. 1a, plates 1–9 dip down near the center but plate 10 does not. Ray tracing showed this causes a radiation "hot spot" just below plate 10 because rays entering the shield between plates 9 and 10 can reach the centerline with fewer reflections than rays entering between lower plates.

Tests indicate that for incident rays that do not bounce clear of the shield after the first reflection, the shield acts almost like a blackbody irrespective of the shield absorptivity. Put another way, ray tracing shows that no matter where a ray goes after initial shield entry, on average, most of its energy will be lost to the shield or to the sensor. This is an undesirable characteristic because the radiative energy absorbed by the shield may eventually cause radiational heating errors.

b. Wind tunnel experiments

Two sets of wind tunnel experiments were conducted: one to measure the flow speed inside the shield and another to measure the temperature rise of a sensor inside the shield as a function of external radiational heating and external flow speed. The National Center for Atmospheric Research (NCAR) wind tunnel was used to evaluate the Gill multiplate shield (as built by R. M. Young) and the N221F shield. Airflow inside the shield, on the vertical shield axis, was measured using a Thermo Systems Inc. model 8470 omnidirectional, hot-film air velocity transducer with a 2-mm-diameter sensing head. The wind profile along the shield axis was measured for various external flow rates starting at 1 m s^{-1}. Excess temperature, air temperature inside the shield minus the air temperature at a point upstream from the shield, was measured using YSI 44006 bead thermistors under various wind speed conditions, while illuminating the shield with a strong light source (projecting 630 w m^{-2} on the shield). Both transducer probes were moved ver-

Tentative empirical straightforward bias correction: Multi-linear regression

Bias =

Cw * Wind

+ Cs * Solar

+ Ca * Cos(solar angle)

+ Intercept

	Estimate	Std error	T-value
Cw (wind)	-0.3	0.01	23
CS (incoming solar)	-1.7E(3	2.E-4	8
Ca (solar angle)	1.9	0.2	12
I (Intercpt)	2.7	0.1	28

- But correction only accounts < 20% total bias
Variance => inefficient

Virtually all AWS reports of atmospheric temperature, and possibly also reports from manned stations, are likely affected

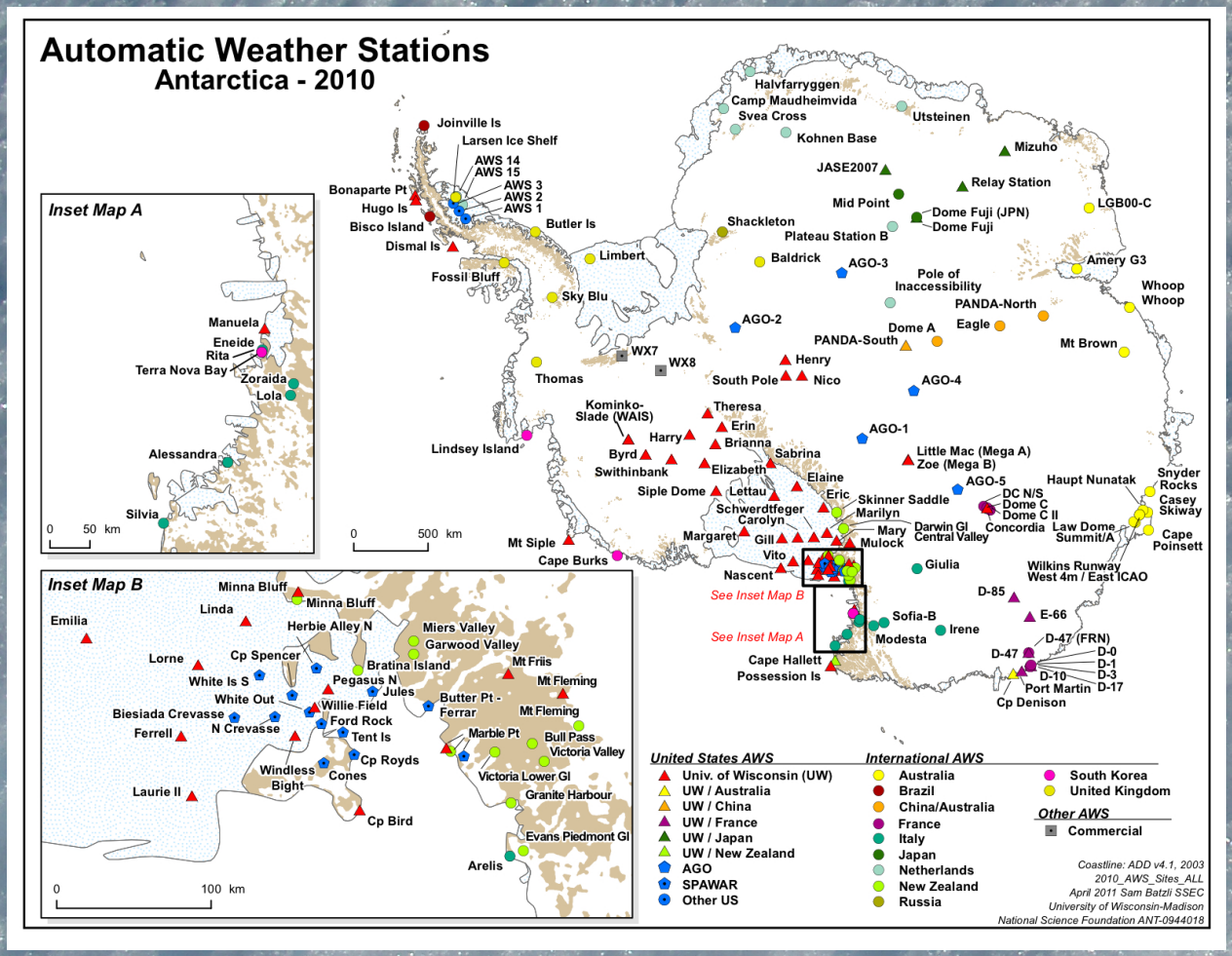

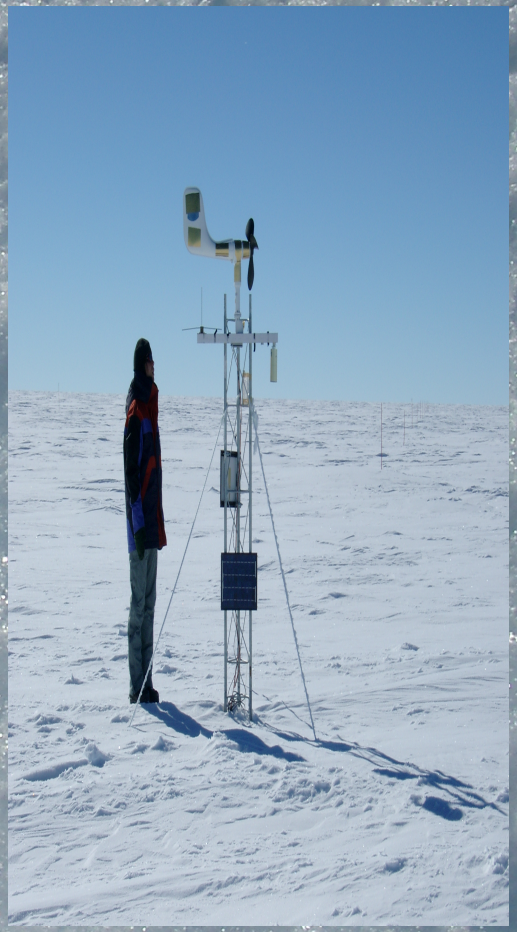

Comparing Dome C AMRC AWS reports with FV measurements

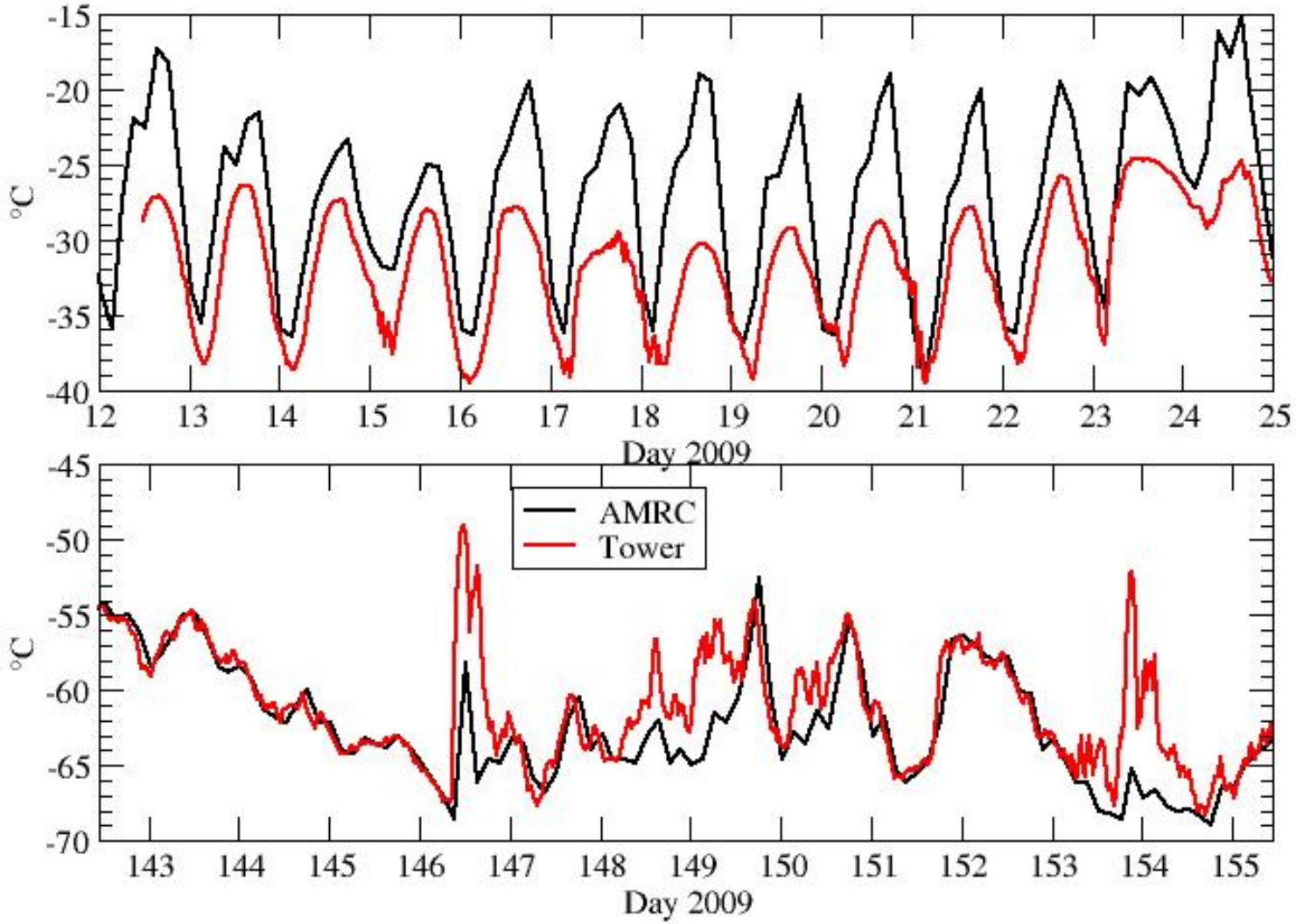

Conclusions:

* Beware of temperature measurement biases in Antarctica !

Conclusions:

* Beware of temperature measurement biases in Antarctica

* Probably less in coastal area (strong frequent catabatic winds)

Conclusions:

* Beware of temperature biases in Antarctica

* Probably less in coastal area (strong frequent catabatic winds)

* No easy universal way to correct

* Better avoid, e.g at measurement. With (apparently) efficient commercially available devices

* Submitted toJournal Atmos. Oceanic Technol.

Conclusions:

* Beware of temperature biases in Antarctica

* Probably less in coastal area (strong frequent catabatic winds)

* No easy universal way to correct

* Better avoid, e.g at measurement. With (apparently) efficient commercially available devices

Submitted toJournal Atmos. Oceanic Technol.

And there are other major issues
with meteorological measurement on the Antarctic plateau: